

# Resummation-based updates for Stochastic Series Expansion Quantum Monte Carlo

Nisheeta Desai<sup>1</sup> and Sumiran Pujari<sup>2,\*</sup>

<sup>1</sup>*Department of Theoretical Physics, Tata Institute of Fundamental Research, Mumbai, India*

<sup>2</sup>*Department of Physics, Indian Institute of Technology Bombay, Mumbai, MH 400076, India*

For spin rotational symmetric models with a positive-definite high-temperature expansion of the partition function, a stochastic sampling of the series expansion upon partial resummation becomes logically equivalent to sampling an uncoloured closely-packed loop-gas model in one higher dimension. We devise quantum Monte Carlo updates based on this for general  $SU(N)$  in fundamental and higher-symmetric representations. The algorithmic performance systematically improves with increase in (continuous)  $N$  allowing efficient simulation of short-loop phases like valence bond solids. The above gives a connection between Sandvik's  $JQ$  model class and classical loop-gas models in the deconfined universality class.

For all areas of physics including strongly correlated matter, efficient computational algorithms are now indispensable. Systematic advances in their design have thus become the keys to progress. Such is exemplarily the case for an important class of algorithms based on the Monte Carlo (MC) method that has provided unbiased insights into multifarious condensed matter systems, as well as lattice gauge theories for elementary particles.

For magnetic insulators that set our backdrop, quantum Monte Carlo (QMC) is now routinely used to study various lattice quantum spin Hamiltonians [1] which provide effective microscopic models for the magnetically active sites in the crystal, or idealized versions aimed at capturing the correct long-distance physics.[2] For these models, an influential set of works [3–8] have set the agenda for charting out the landscape of magnetic and, importantly, quantum non-magnetic phases and associated quantum phase transitions. The large- $N$  perturbative approach of Refs. [3, 5–8] offers insights into  $SU(2)$  magnets [9], and also connects to quantum dimer models[10] in the  $N \rightarrow \infty$  limit that serve as effective low-energy models for spin systems[6].

There are two well-known flavors of QMC for simulating these spin models on a  $d$ -dimensional lattice at finite temperatures that are extremely efficient for small  $N$ . One is based on a path-integral representation in  $d + 1$  dimensions in (imaginary) time[11, 12], and the other based on a stochastic sampling of the high-temperature series expansion (SSE) of the partition function which leads to a discrete  $(d+1)$ -dimensional formulation.[13, 14] Both approaches share a close relation — as a simple example, there is a well-defined spin state on the lattice ( $\prod_{i \in \text{lattice}} \otimes |s_i^z\rangle$ ) at any point or slice in the additional dimension in both representations —, and the ideas in one context may be ported into the other.[15] There are also zero-temperature ( $T = 0$ ) projection-based QMC methods that stochastically project out the ground state from a trial state by exploiting the valence bond basis for antiferromagnetic ground states in the singlet sector [16] including a continuous- $N$  generalization [17].

What has made these methods really powerful is the loop algorithm[12, 18–23] and its extensions[24–31] which

perform non-local updates similar to cluster updates in classical lattice simulations.[32, 33] The loop algorithm is based on a colored loop representation of the partition function [34], and changing the color of loops leads to non-local updates. This idea can be used in  $T = 0$  valence bond projector-QMC as well by reintroducing spin variables judiciously in the valence bond formulation as shown by Sandvik and Evertz [23], which also works for Beach *et al*'s continuous- $N$  generalization. [35] Such loop color updates have also been exploited to study classical loop gas models [36–38] whose universal properties can parallel that of spin models. This connection goes the other way too, i.e. spin models at finite- $T$  may be converted to classical (uncolored) loop models in one higher dimension as noted in “Suzuki-Trotterized” contexts. [22, 39, 40] This is essentially a resummation over the spin variables.

In this work, we design finite- $T$  non-local SSE updates based on this resummation which directly handle uncolored loops without any reference to the underlying spin states. This takes advantage of the basic SSE setup which incurs no Suzuki-Trotter errors[41]. These updates lead to a systematic improvement in algorithmic performance as  $N$  increases. In relation to the classical loop-gas models alluded to above[36–38], the resultant algorithm is well-suited for simulations of phases with predominantly short loops. In fact, this pure loop formulation generalizes the essential idea of valence bond  $T = 0$  projector-QMC method via the resummation-based updates to simultaneously access both finite temperatures and any total spin sector. More broadly speaking, uncolored short-loops in space-time are rather the natural objects or building blocks for quantum non-magnetic phases like valence bond solids. These states are of long-standing interest both intrinsically, and for possible proximity to spin-liquid states. On the other hand, colored loops with definite spin states are the natural objects in long-loop phases which correspond to magnetic phases that was exploited by Sandvik-Evertz. [23] We also combine the above with the SSE methods developed by one of the authors in Ref. [42, 43] for efficient simulation of higher-symmetric representations of  $SU(N)$  that were in-

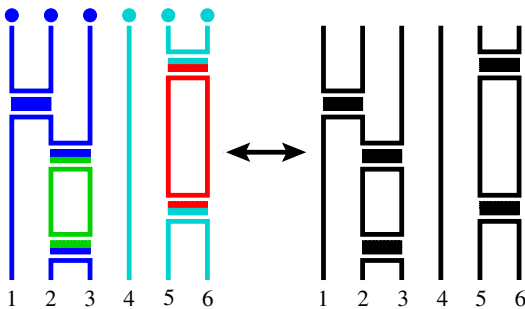


FIG. 1. Illustrative operator string configurations for standard SSE (left) with definite spin states, and for resummed SSE (right) characterized purely by uncolored loops.

roduced by Read and Sachdev [6] to expose the myriad possible quantum non-magnetic states for higher spins.

*Fundamental representation:*– We describe the basic idea using the canonical  $SU(2)$  spin- $\frac{1}{2}$  nearest neighbor Heisenberg Hamiltonian on a bipartite lattice. It is

$H = J \sum_{\langle i,j \rangle} \mathbf{s}_i \cdot \mathbf{s}_j$  where  $\mathbf{s}_i \equiv (s_i^x, s_i^y, s_i^z)$  are spin- $\frac{1}{2}$  operators on site  $i$  at position  $\mathbf{r}_i$ , and  $\langle i, j \rangle$  indexes the nearest-neighbor bonds of the lattice. After a sublattice unitary rotation,  $H = -J \sum_{\langle i,j \rangle} H_{ij}$  with the “singlet projector”  $H_{ij} = \frac{1}{N} \sum_{\alpha, \beta} |\alpha_i \alpha_j\rangle \langle \beta_i \beta_j|$  up to an innocuous constant.  $\alpha, \beta$  range from 1 to  $N = 2$ [44, 45]. Then, the high-temperature series representation of the partition function  $Z(\beta) = \text{Tr}(e^{-\beta H}) = \sum_n \frac{(-\beta)^n}{n!} \text{Tr}(H^n)$  with  $\beta \equiv \frac{1}{kT}$  becomes the (positive-definite) operator-string representation of SSE:

$$\sum_{n=0}^{\infty} \frac{(-\beta)^n}{n!} \sum_{S_n} \sum_{\alpha} \langle \alpha | H_{\{b_1, \mu_1\}} H_{\{b_2, \mu_2\}} \dots H_{\{b_n, \mu_n\}} | \alpha \rangle$$

where  $S_n$  denotes a string of operator indices, and  $\{b_m, \mu_m\}$  is a joint index that tracks for the  $m^{\text{th}}$  operator in the operator string its bond location  $\langle i, j \rangle$  where  $H_{ij}$  “lives” via  $b_m$ , and whether it is diagonal or off-diagonal in the usual choice of  $s^z$  basis via  $\mu_m$ . The operator-string representation thus lives in  $d + 1$  dimensions. As remarked earlier, it can be imagined as a configuration of closely-packed coloured loops[34] as shown in Fig. 1(a). Now, one may resum over the spin or colour values of these closely-packed loops without breaking or changing any loop connections in the operator string. This then renders the ensemble as a configuration of closely-packed uncoloured loops as shown in Fig. 1(b). This loop-gas representation for the high-temperature series may be written as

$$Z(\beta) = \sum_{n=0}^{\infty} \frac{(-\beta)^n}{n!} N^{n_l} \sum_{S_n} h_{b_1} h_{b_2} \dots h_{b_n} \quad (1)$$

where bond index  $b_i$  is now the only indexing required,  $h_{b_i}$  indicates the spin-symmetric matrix element contribution ( $-\frac{J}{N}$  in our example) at  $b_i$ , and  $n_l$  is the number of loops in a given configuration.

We may suggestively rewrite the above as  $Z = \sum_{\{C_{\text{loops}}\}} W(C_{\text{loops}})$  where  $C_{\text{loops}}$  is any allowed closely-packed uncoloured loop gas configuration with only one underlying operator where two loops abut each other at various time slices (Fig. 1(b)), and  $W(C_{\text{loops}}) = \frac{(\beta J/N)^n}{n!} N^{n_l}$ . The underlying operators thus perform the role of “transfer matrices” in the loop-gas language [36]. The uncolored nature of the loop-gas emerges in presence of  $SU(N)$  symmetry, which ensures that the diagonal and off-diagonal operators contribute the same factor to the weight of the configuration. Having done the resummation though,  $N$  is now purely a parameter and can be any positive, real number. It also gets rid of the index which tracks diagonal vs. off-diagonal operators, which implies a superposition of spin states at any time slice.

*Estimators:*– The simplest QMC estimator is energy, and it is measured in the same way here as in standard SSE. This is because, if we now color back the uncolored loops, the contribution to the energy estimator is *independent* of the coloring, i.e. each coloring contributes the same value ( $\frac{n}{\beta}$ ) to the energy estimator. [15] The measurement of bond operators also remains unchanged, e.g.  $B_{\lambda}(\vec{r}) \equiv \mathbf{s}_{\mathbf{r}} \cdot \mathbf{s}_{\mathbf{r}+\hat{e}_{\lambda}}$  on the square lattice. We can similarly measure the square lattice VBS order parameters,  $\phi_x = \frac{1}{N_s} \sum_{\mathbf{r}} (-1)^{r_x} \langle B_x(\mathbf{r}) \rangle$  and  $\phi_y = \frac{1}{N_s} \sum_{\mathbf{r}} (-1)^{r_y} \langle B_y(\mathbf{r}) \rangle$ . Measuring the correlations of the bond operator  $\tilde{C}_{\phi_{\lambda}}(\mathbf{r}) = \langle B_{\lambda}(\mathbf{0}) B_{\lambda}(\mathbf{r}) \rangle$  is also straightforward. The estimator of the spin stiffness which tracks magnetic ordering is changed due to the resummation. In standard SSE, the stiffness is related to the winding of colored loops according to the following relation  $\rho = \frac{\langle \mathcal{W}_c^2 \rangle}{\beta}$ , where  $\langle \mathcal{W}_c^2 \rangle$  is the winding fluctuations of colored loops. [15] It is related to the winding fluctuations of uncolored loops as  $\langle \mathcal{W}_u^2 \rangle = \frac{N^2}{(N-1)} \langle \mathcal{W}_c^2 \rangle$  which gives an “improved” estimator for the stiffness:

$$\rho = \frac{(N-1)}{N^2} \frac{\langle \mathcal{W}_u^2 \rangle}{\beta}. \quad (2)$$

The derivation of the winding fluctuation relation is given in Ref.[46]. This estimator for stiffness can be used in standard SSE as well.

*Implementation and Application:*– Based on Eq. 1, we implement a Monte Carlo algorithm to directly sample the uncoloured loop ensemble. The proposal consists in inserting a spin-symmetric operator at an “identity” location or removing an already existing “non-identity” spin-symmetric operator at various space-time locations. The proposals get accepted with Metropolis probabilities which are governed by the change  $n \rightarrow n \pm 1$  (for Heisenberg model) and the change in the number of loops  $\delta(n_l)$ . [46] For  $H_{ij}$ ,  $\delta(n_l)$  takes only the values  $\pm 1$  purely due to considerations of loop topology.

One may anticipate improved performance as  $N$  increases compared to standard SSE, because off-diagonal operator contributions in standard SSE operator string

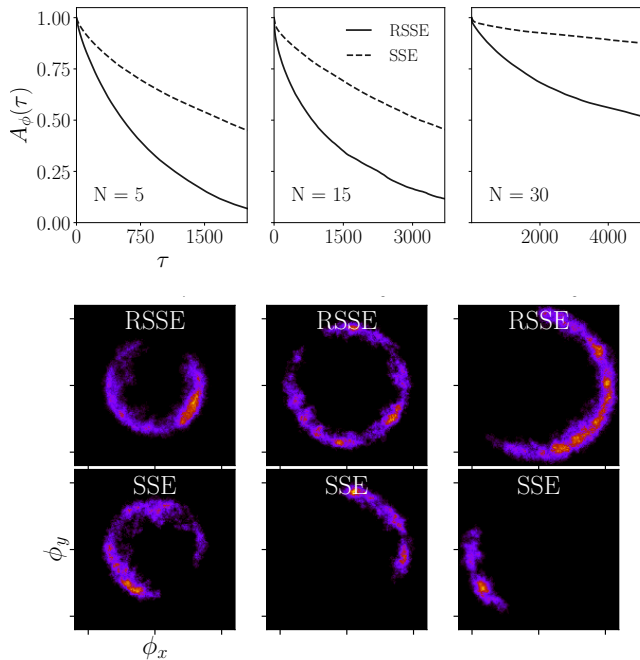


FIG. 2. (top) Comparison of autocorrelation of the VBS order parameter ( $\phi = \sqrt{\phi_x^2 + \phi_y^2}$ ) on a  $16 \times 16$  lattice for  $N = 5, 15, 30$  measured after each Monte Carlo step using the resummation algorithm with that of the standard SSE. Autocorrelations fall off faster in the resummed SSE (RSSE) algorithm systematically as  $N$  increases. These values of  $N$  correspond to the short-loop or VBS phase[47] showing the efficacy of resummation-based updates for short-loop phases in general. (bottom) Joint histograms of the VBS order parameters,  $\phi_x$  and  $\phi_y$ , on a  $16 \times 16$  lattice.  $\phi_x$  and  $\phi_y$  have been measured at every Monte Carlo step for  $10^6$  steps. For  $N = 7$ , the performance of both algorithms are comparable. However, as we go deeper into the VBS phase for higher values of  $N$ , we clearly see that resummed SSE (RSSE) spans the angular space of the histogram better, thus proving to be the more ergodic algorithm in this regime.

start to dominate those of diagonal operators as  $N$  increases. This makes the “diagonal” update of standard SSE – that changes  $n$  by inserting or removing diagonal operators between two definite spin states – less efficient in updating the operator string (the “off-diagonal” update of standard SSE changes only the spin or color value of the loop as remarked earlier, and does not change  $n$ ). This is a non-issue in our algorithm; operators can be potentially inserted or removed at any space-time location. This improved performance is indeed seen as discussed in Fig. 2. From a loop-gas perspective, the resummed SSE algorithm is apt for simulating any phase with predominantly short loops where the computation of  $\delta(n_i)$  becomes quite efficient. Thus, it is preferable for short-loop phases like valence bond solids (Fig. 2) as mentioned earlier. This should apply for other non-magnetic phases like the plaquette or the Haldane-nematic phase. [7, 48] These updates can also supplement the standard SSE

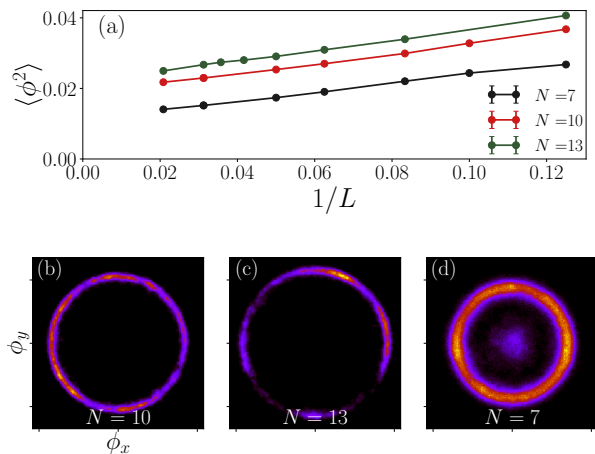


FIG. 3. (a) Finite size scaling of the VBS order parameter for the  $SU(N)$  square lattice antiferromagnet in the fundamental representation for  $N = 7, 10, 13$  at  $\beta = 128$  (representative of zero-temperature limit [46]). It clearly extrapolates to finite values showing VBS order in this regime as is expected[47]. (bottom) The joint histogram of  $\phi_x$  and  $\phi_y$  measured at every  $10^{\text{th}}$  Monte Carlo step with a total of  $10^7$  steps. (b)-(c) At  $\beta = 128$ , the histograms show  $U(1)$  symmetry for  $N = 10, 13$  on a  $32 \times 32$  lattice. (d) For  $N = 7$ , at  $\beta = 64$  on a  $16 \times 16$  lattice, the distribution peaks at an  $U(1)$  symmetric ring and at  $\phi_x = \phi_y = 0$  suggesting a first-order transition.

diagonal and loop updates in long-loop phases or near transitions if needed for performance.

We now apply the resummed SSE algorithm to the square lattice antiferromagnet for several  $N$ . In the fundamental representation, it maps to the non-interacting quantum dimer model (QDM) with one dimer per vertex as  $N \rightarrow \infty$ [6]. Only very recently, an efficient algorithm based on SSE has been developed for finite- $T$  simulations directly in the constrained Hilbert space of the QDM.[49] We can also access the large- $N$  regime in our simulations efficiently. In Fig. 3(a), we see VBS order at low enough temperatures in this regime. However, we see  $U(1)$ -symmetric VBS order histograms as shown in Fig. 3(b,c) in contrast to the “mixed” phase histograms of Ref.[50] for similar system sizes. The approach to the constrained Hilbert space of QDM in the loop gas representation can also be quantified [46]. We find non-negligible deviations from QDM Hilbert space to put  $SU(N)$  magnets away from the perturbative neighborhood of QDM even for quite large  $N$ . We ascribe this to the contrast between our results and Ref.[50] – a relevant detail on the connection between  $SU(N)$  magnets and QDM. Fig. 3(d) shows how the algorithm performs near the thermal transition out of the ordered phase.

*Higher symmetric representations:*– We now write down resummation-based updates for higher representations by making use of the “split-spin” language[40, 42, 51, 52] which splits  $\mathbf{S}_i$  as  $\mathcal{P}_i \left( \sum_{a=1}^{2S} \mathbf{s}_{i,a} \right) \mathcal{P}_i$  where  $\mathcal{P}_i$  are appropriate projection operators to stay in the

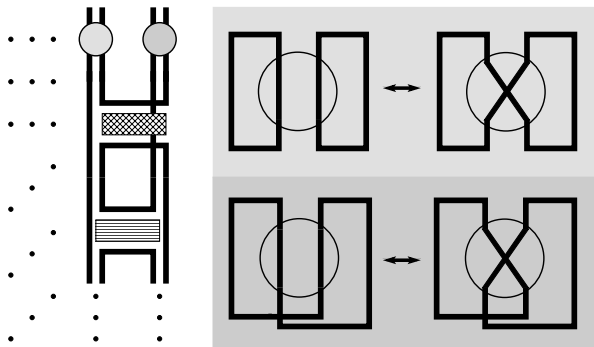


FIG. 4. Schematic to illustrate the resummation over the projection operators. On the left side is shown a small section of the uncolored loop QMC configuration with two split-spins per site. On the right is shown the re-wiring MC update at the projection time slice. The shade of gray corresponds to the projection operators shown as circles in the QMC configuration on the left, assuming a loop geometry without any other operators on the shown bond elsewhere in time.

correct Hilbert space. We take the spin-1 Heisenberg model for  $SU(2)$  as our example, which automatically extends to the  $SU(N)$  case with two symmetric “flavours”. The spin-1 Heisenberg model  $H = J \sum_{\langle i,j \rangle} (\mathbf{S}_i \cdot \mathbf{S}_j)$  in the split-spin language is written as  $H = \mathcal{P} \tilde{H} \mathcal{P}$  with  $\tilde{H} = J \sum_{\langle i,j \rangle} \sum_{a,b} \mathbf{s}_{i,a} \cdot \mathbf{s}_{j,b}$  and  $a, b$  is now a split-spin index running over the number of symmetric flavors.  $\mathcal{P}$  is a projection operator that projects onto fully symmetric subspace over the split-spins, i.e.  $\mathcal{P} = \prod_i \mathcal{P}_i$  and  $\mathcal{P}_i \equiv |\uparrow\uparrow\rangle\langle\uparrow\uparrow| + |\downarrow\downarrow\rangle\langle\downarrow\downarrow| + \frac{(|\uparrow\downarrow\rangle + |\downarrow\uparrow\rangle)}{\sqrt{2}} \frac{(|\uparrow\downarrow\rangle + |\downarrow\uparrow\rangle)}{\sqrt{2}}$  for the two split-spins on the  $i^{\text{th}}$  site. With this in hand, the standard-SSE operator-string representation follows from  $Z(\beta) = \text{Tr}_{\mathbf{S}} (e^{-\beta H}) = \text{Tr}_{\mathbf{S}} (e^{-\beta \tilde{H} \mathcal{P}})$ . To ensure symmetrization, it is enough that the projection operator acts at one particular time slice. [51] We may now resum as before to get a configuration in terms of uncoloured loops, but now there will be two “parallel” loops running at each space-time point as sketched on the left side of Fig.4. The resummation over colours proceeds exactly the same as before to give the  $N^{n_l}$  re-weighting factor.

To resum over the projection operator, one must ensure that the action of the projection operator  $\mathcal{P}_i$  is faithfully captured on all sites. In standard SSE, one implements the projection by the use of a directed loop update[25, 27] at the projection time slice.[53] Resumming over this now amounts to a “re-wiring” of the two uncolored loops at the two split-spin sites at this time slice as shown on the right side of Fig. 4. So, the implementation essentially mimics that of the earlier section with an extra MC update for the projection time slice where one proposes to reconfigure the split-spin connections as in Fig. 4 with the acceptance probability again governed by the  $\delta(n_l)$  due to this proposal.[46] Extending this to yet higher-symmetric representations follows along very similar lines with more

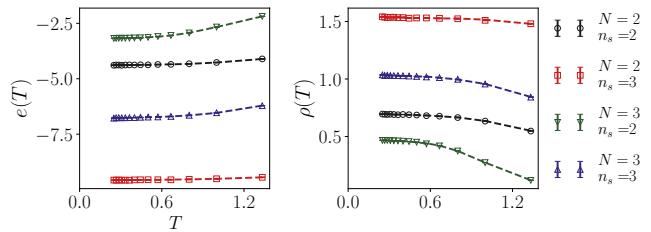


FIG. 5. Comparison of finite temperature energy per unit site,  $e(T)$ , and spin stiffness,  $\rho(T)$ , measured in our algorithm with standard SSE (dashed lines) on a  $4 \times 4$  lattice for several  $N$  and  $n_s$  (number of split-spins or symmetric flavors).

split-spins per site. In Fig. 5, we demonstrate the implementation of these extensions by benchmarking energy and spin stiffness with standard SSE. This provides an alternative to standard SSE that can allow more efficient access to the quantum non-magnetic states of  $SU(N)$  antiferromagnets [6, 7] thereby opening up further studies on (quantum) phase transitions with  $N$  and  $T$ . [54]

*Discussion:*— One may finally ask if there is a physical meaning to the uncolored loops, or are they just algorithmic constructs. Any such interpretation, apart from providing intuition, can help formulate other useful QMC estimators [55] based on our generalization of the valence bond  $T = 0$  projector-QMC method to finite- $T$  without the singlet sector restriction. We can indeed interpret them as follows: at a coloured level in standard SSE, an operator  $|\alpha_i \alpha_j\rangle \langle \beta_i \beta_j|$  destroys  $\beta_i, \beta_j$  in a state (“below” the operator in Fig. 1) and creates  $\alpha_i, \alpha_j$  in the resultant state (“above” the operator). Thus,  $|\alpha_i \alpha_j\rangle \langle \beta_i \beta_j| \equiv b_{i,\alpha}^\dagger b_{j,\alpha}^\dagger b_{i,\beta} b_{j,\beta}$  where  $b, b^\dagger$  stand for the destruction and creation operations respectively. If  $\chi_{ij,\alpha} \equiv b_{i,\alpha} b_{j,\alpha}$ , then an  $\alpha$ -colored loop is of the form  $\chi_{l_i,\alpha}^\dagger \dots \chi_{j_k,\alpha}^\dagger \chi_{ij,\alpha}$ . Therefore, upon resumming, an uncolored loop has the following  $SU(N)$ -symmetric operator content:  $\tilde{\chi}_{l_i}^\dagger \dots \tilde{\chi}_{j_k}^\dagger \tilde{\chi}_{ij}$  with  $\tilde{\chi}_{ij} = \sum_{\alpha} \chi_{ij,\alpha}$ . A similar interpretation in the “reverse” direction from loops to magnetic degrees of freedom was laid down by Nahum *et al* in Refs.[36, 37, 56], but the Hamiltonian does not take a simple form for  $3d$  loop-gases[57]. Resummation instead gives a recipe to go from local Hamiltonians to loop-gases including for higher-symmetric representations.

The above interpretation gives a connection between the  $2d$   $JQ$  models[2, 58] and the  $3d$  loop-gas model studied by Nahum *et al* in Ref.[38] both of which have been argued to exhibit deconfined criticality[59, 60]. The  $Q$  term – a tensor product of several singlet projectors over independent bonds  $\prod_{i=1}^p H_{b_i}$  – gives an additional rule for how loops may abut each other on a given time slice. A  $Q$ -operator in the uncolored loop representation will lead to  $p$  loop pairs to touch at a given time slice of the layered extension of the underlying lattice, just as a single  $H_b$  led to a single loop pair to touch as in Fig. 1. The  $J, Q$  terms in the loop-gas language thus

define appropriate transfer matrices. This throws a “forward” perspective on Ref.[38, 61], in that by resumming, any spin-symmetric Hamiltonian with a positive-definite high-temperature series expansion exhibiting deconfined criticality implies the same between a long-loop and a short-loop phase in a logically equivalent loop-gas.

*Acknowledgements:*– We thank Fabien Alet, Kedar Damle and Ribhu Kaul for discussions. We especially thank Kedar Damle for a critical reading and feedback on the manuscript. N.D. was partially supported by NSF grant DMR-1611161, and partially by a National Postdoctoral Fellowship of SERB, DST, Govt. of India (PDF/2020/001658) at the Dept of Theoretical Physics TIFR. S.P. was supported by IRCC, IIT Bombay (17IR-CCSG011) and SERB, DST, India (SRG/2019/001419).

---

\* sumiran@phy.iitb.ac.in

- [1] A. W. Sandvik, Autumn School on Correlated Electrons, Jülich (Germany), 16 Sep 2019 - 20 Sep 2019 (Forschungszentrum Jülich GmbH Zentralbibliothek, Verlag, Jülich, 2019), vol. 9 of *Schriften des Forschungszentrums Jülich. Modeling and Simulation*, pp. 16.1–16.32, ISBN 978-3-95806-400-3, URL <https://juser.fz-juelich.de/record/864818>.
- [2] R. K. Kaul, R. G. Melko, and A. W. Sandvik, Annual Review of Condensed Matter Physics **4**, 179 (2013), <https://doi.org/10.1146/annurev-conmatphys-030212-184215>, URL <https://doi.org/10.1146/annurev-conmatphys-030212-184215>.
- [3] I. Affleck, Phys. Rev. Lett. **54**, 966 (1985), URL <https://link.aps.org/doi/10.1103/PhysRevLett.54.966>.
- [4] F. D. M. Haldane, Phys. Rev. Lett. **61**, 1029 (1988), URL <https://link.aps.org/doi/10.1103/PhysRevLett.61.1029>.
- [5] N. Read and S. Sachdev, Phys. Rev. Lett. **62**, 1694 (1989), URL <https://link.aps.org/doi/10.1103/PhysRevLett.62.1694>.
- [6] N. Read and S. Sachdev, Nuclear Physics B **316**, 609 (1989), ISSN 0550-3213, URL <https://www.sciencedirect.com/science/article/pii/0550321389900618>.
- [7] N. Read and S. Sachdev, Phys. Rev. B **42**, 4568 (1990), URL <https://link.aps.org/doi/10.1103/PhysRevB.42.4568>.
- [8] N. Read and S. Sachdev, Phys. Rev. Lett. **66**, 1773 (1991), URL <https://link.aps.org/doi/10.1103/PhysRevLett.66.1773>.
- [9] Also,  $SU(N)$  or, more generally,  $SU(2) \otimes SU(M)$  arise physically for Kugel-Khomskii models with both spin and orbital degrees of freedom, and other contexts with additional internal quantum numbers. The algorithmic ideas in this paper extend quite naturally to these models as well.
- [10] D. S. Rokhsar and S. A. Kivelson, Phys. Rev. Lett. **61**, 2376 (1988), URL <https://link.aps.org/doi/10.1103/PhysRevLett.61.2376>.
- [11] M. Suzuki, S. Miyashita, and A. Kuroda, Progress of Theoretical Physics **58**, 1377 (1977), ISSN 0033-068X, <https://academic.oup.com/ptp/article-pdf/58/5/1377/5389651/58-5-1377.pdf>, URL <https://doi.org/10.1143/PTP.58.1377>.
- [12] B. B. Beard and U.-J. Wiese, Phys. Rev. Lett. **77**, 5130 (1996), URL <https://link.aps.org/doi/10.1103/PhysRevLett.77.5130>.
- [13] A. W. Sandvik and J. Kurkijärvi, Phys. Rev. B **43**, 5950 (1991), URL <https://link.aps.org/doi/10.1103/PhysRevB.43.5950>.
- [14] A. W. Sandvik, Journal of Physics A: Mathematical and General **25**, 3667 (1992), URL <https://doi.org/10.1088/0305-4470/25/13/017>.
- [15] A. W. Sandvik, in *Lectures on the Physics of Strongly Correlated Systems Xiv: Fourteenth Training Course in the Physics of Strongly Correlated Systems*, edited by A. Avella and F. Mancini (2010), vol. 1297 of *American Institute of Physics Conference Series*, pp. 135–338, 1101.3281.
- [16] A. W. Sandvik, Phys. Rev. Lett. **95**, 207203 (2005), URL <https://link.aps.org/doi/10.1103/PhysRevLett.95.207203>.
- [17] K. S. D. Beach, F. Alet, M. Mambrini, and S. Capponi, Phys. Rev. B **80**, 184401 (2009), URL <https://link.aps.org/doi/10.1103/PhysRevB.80.184401>.
- [18] H. G. Evertz, G. Lana, and M. Marcu, Phys. Rev. Lett. **70**, 875 (1993), URL <https://link.aps.org/doi/10.1103/PhysRevLett.70.875>.
- [19] H.-P. Ying, U.-J. Wiese, and D.-R. Ji, Physics Letters A **183**, 441 (1993), ISSN 0375-9601, URL <https://www.sciencedirect.com/science/article/pii/037596019390603W>.
- [20] N. Kawashima and J. E. Gubernatis, Phys. Rev. Lett. **73**, 1295 (1994), URL <https://link.aps.org/doi/10.1103/PhysRevLett.73.1295>.
- [21] A. W. Sandvik, Phys. Rev. B **59**, R14157 (1999), URL <https://link.aps.org/doi/10.1103/PhysRevB.59.R14157>.
- [22] H. G. Evertz, Advances in Physics **52**, 1 (2003), <https://doi.org/10.1080/0001873021000049195>, URL <https://doi.org/10.1080/0001873021000049195>.
- [23] A. W. Sandvik and H. G. Evertz, Phys. Rev. B **82**, 024407 (2010), URL <https://link.aps.org/doi/10.1103/PhysRevB.82.024407>.
- [24] N. V. Prokof'ev, B. V. Svistunov, and I. S. Tupitsyn, Journal of Experimental and Theoretical Physics **87**, 310 (1998), ISSN 1090-6509, URL <https://doi.org/10.1134/1.558661>.
- [25] O. F. Syljuåsen and A. W. Sandvik, Phys. Rev. E **66**, 046701 (2002), URL <https://link.aps.org/doi/10.1103/PhysRevE.66.046701>.
- [26] A. W. Sandvik, Phys. Rev. E **68**, 056701 (2003), URL <https://link.aps.org/doi/10.1103/PhysRevE.68.056701>.
- [27] F. Alet, S. Wessel, and M. Troyer, Phys. Rev. E **71**, 036706 (2005), URL <https://link.aps.org/doi/10.1103/PhysRevE.71.036706>.
- [28] D. Heidarian and K. Damle, Phys. Rev. Lett. **95**, 127206 (2005), URL <https://link.aps.org/doi/10.1103/PhysRevLett.95.127206>.
- [29] S. V. Isakov, S. Wessel, R. G. Melko, K. Sengupta, and Y. B. Kim, Phys. Rev. Lett. **97**, 147202 (2006), URL <https://link.aps.org/doi/10.1103/PhysRevLett.97.147202>.
- [30] R. G. Melko, Journal of Physics: Condensed Matter

- 19, 145203 (2007), URL <https://doi.org/10.1088/0953-8984/19/14/145203>.
- [31] S. Biswas, G. Rakala, and K. Damle, Phys. Rev. B **93**, 235103 (2016), URL <https://link.aps.org/doi/10.1103/PhysRevB.93.235103>.
- [32] R. H. Swendsen and J.-S. Wang, Phys. Rev. Lett. **58**, 86 (1987), URL <https://link.aps.org/doi/10.1103/PhysRevLett.58.86>.
- [33] U. Wolff, Phys. Rev. Lett. **62**, 361 (1989), URL <https://link.aps.org/doi/10.1103/PhysRevLett.62.361>.
- [34] R. K. Kaul, Phys. Rev. B **91**, 054413 (2015), URL <https://link.aps.org/doi/10.1103/PhysRevB.91.054413>.
- [35] See footnote [19] of Beach *et al* [17], and the associated text.
- [36] A. Nahum, J. T. Chalker, P. Serna, M. Ortuño, and A. M. Somoza, Phys. Rev. Lett. **107**, 110601 (2011), URL <https://link.aps.org/doi/10.1103/PhysRevLett.107.110601>.
- [37] A. Nahum, J. T. Chalker, P. Serna, M. Ortuño, and A. M. Somoza, Phys. Rev. B **88**, 134411 (2013), URL <https://link.aps.org/doi/10.1103/PhysRevB.88.134411>.
- [38] A. Nahum, J. T. Chalker, P. Serna, M. Ortuño, and A. M. Somoza, Phys. Rev. X **5**, 041048 (2015), URL <https://link.aps.org/doi/10.1103/PhysRevX.5.041048>.
- [39] M. Aizenman and B. Nachtergaele, Communications in Mathematical Physics **164**, 17 (1994), ISSN 1432-0916, URL <https://doi.org/10.1007/BF02108805>.
- [40] N. Kawashima and J. E. Gubernatis, Journal of Statistical Physics **80**, 169 (1995), ISSN 1572-9613, URL <https://doi.org/10.1007/BF02178358>.
- [41] M. Suzuki, Progress of Theoretical Physics **56**, 1454 (1976), ISSN 0033-068X, <https://academic.oup.com/ptp/article-pdf/56/5/1454/5264429/56-5-1454.pdf>, URL <https://doi.org/10.1143/PTP.56.1454>.
- [42] N. Desai and R. K. Kaul, Phys. Rev. Lett. **123**, 107202 (2019), URL <https://link.aps.org/doi/10.1103/PhysRevLett.123.107202>.
- [43] N. Desai, Ph.D. thesis, University of Kentucky, Lexington, KY, USA (2020).
- [44] R. K. Kaul, Phys. Rev. B **84**, 054407 (2011), URL <https://link.aps.org/doi/10.1103/PhysRevB.84.054407>.
- [45] Formally, for  $N > 2$ , the magnetic degrees of freedom are in the fundamental representation on one sublattice, while they are in the conjugate-to-fundamental representation on the other sublattice. See e.g. Ref. 44.
- [46] See supplementary document for further details on the implementation of the resummation-based updates, and some other technical details. Also, the final section discusses the approach to the quantum dimer model Hilbert space in the large- $N$  regime for the uncolored loop representation.
- [47] K. Harada, N. Kawashima, and M. Troyer, Phys. Rev. Lett. **90**, 117203 (2003), URL <https://link.aps.org/doi/10.1103/PhysRevLett.90.117203>.
- [48] I. Affleck, T. Kennedy, E. H. Lieb, and H. Tasaki, Communications in Mathematical Physics **115**, 477 (1988), ISSN 1432-0916, URL <https://doi.org/10.1007/BF01218021>.
- [49] Z. Yan, Y. Wu, C. Liu, O. F. Syljuåsen, J. Lou, and Y. Chen, Phys. Rev. B **99**, 165135 (2019), URL <https://link.aps.org/doi/10.1103/PhysRevB.99.165135>.
- [50] Z. Yan, Z. Zhou, O. F. Syljuåsen, J. Zhang, T. Yuan, J. Lou, and Y. Chen, Phys. Rev. B **103**, 094421 (2021), URL <https://link.aps.org/doi/10.1103/PhysRevB.103.094421>.
- [51] S. Todo and K. Kato, Phys. Rev. Lett. **87**, 047203 (2001), URL <https://link.aps.org/doi/10.1103/PhysRevLett.87.047203>.
- [52] N. Kawashima and K. Harada, Journal of the Physical Society of Japan **73**, 1379 (2004), <https://doi.org/10.1143/JPSJ.73.1379>, URL <https://doi.org/10.1143/JPSJ.73.1379>.
- [53] See supplementary of Ref. 42.
- [54] Zero temperature projector variants of the resummed SSE algorithm in higher symmetric representations can also now be envisaged.
- [55] K. Beach and A. W. Sandvik, Nuclear Physics B **750**, 142 (2006), ISSN 0550-3213, URL <https://www.sciencedirect.com/science/article/pii/S0550321306004214>.
- [56] See in particular Sec. IIIA of Ref. 37.
- [57] See in particular Sec. IIID of Ref. 37.
- [58] A. W. Sandvik, Phys. Rev. Lett. **98**, 227202 (2007), URL <https://link.aps.org/doi/10.1103/PhysRevLett.98.227202>.
- [59] T. Senthil, A. Vishwanath, L. Balents, S. Sachdev, and M. P. A. Fisher, Science **303**, 1490 (2004), ISSN 0036-8075, <https://science.sciencemag.org/content/303/5663/1490.full.pdf>, URL <https://science.sciencemag.org/content/303/5663/1490>.
- [60] T. Senthil, L. Balents, S. Sachdev, A. Vishwanath, and M. P. A. Fisher, Phys. Rev. B **70**, 144407 (2004), URL <https://link.aps.org/doi/10.1103/PhysRevB.70.144407>.
- [61] In Ref. 38, the underlying lattice of the classical loop gas is the so-called “3D L lattice” (Fig. 1 of Ref. 38), while the  $JQ$  model on square lattice maps to a loop gas on a simple cubic lattice. Such a difference is expected to not affect the long-distance universal physics, since both lattice have the same cubic symmetry. Same goes for the microscopic differences in the transfer matrices.

# Supplemental Material

## DETAILS OF THE ALGORITHM

Our algorithm samples configurations of a closely-packed uncolored loop gas ensemble as explained in the main text. For convenience, we take the standard step of working with operator strings of fixed-length,  $M$ , where the Hamiltonian operators are padded with identities (e.g. see Eqns. 258,263 of [1]). Thus, the partition function can be re-written as

$$Z(\beta) = \sum_{S_M} \frac{(M-n)!}{M!} (-\beta)^n N^{n_l} h_{b_1} h_{b_2} \dots h_{b_M} \quad (1)$$

where  $n$  refers to the number of non-identity Hamiltonian operators,  $S_M$  is the fixed-length operator string with  $n$  non-identities and  $M-n$  identities,  $h_{b_i}$  is either the spin-symmetric matrix element or an identity matrix element, and the sum over  $S_M$  implicitly includes the sum over  $n$  in the main text. Therefore, for our example of  $H = -J \sum_{\langle i,j \rangle} H_{ij}$  with  $H_{ij} = \frac{1}{N} \sum_{\alpha} |\alpha_i \alpha_j\rangle \langle \alpha_i \alpha_j|$ , the Monte Carlo weight of a configuration with  $n$  number of non-identities and  $n_l$  number of loops in the configuration is given by:

$$W(n, M, n_l) = \left(\frac{\beta J}{N}\right)^n \frac{(M-n)!}{M!} N^{n_l} \quad (2)$$

This is the weight of an operator string in standard fixed-length SSE [1] multiplied by the number of possible colorings of  $n_l$  loops,  $N^{n_l}$ .

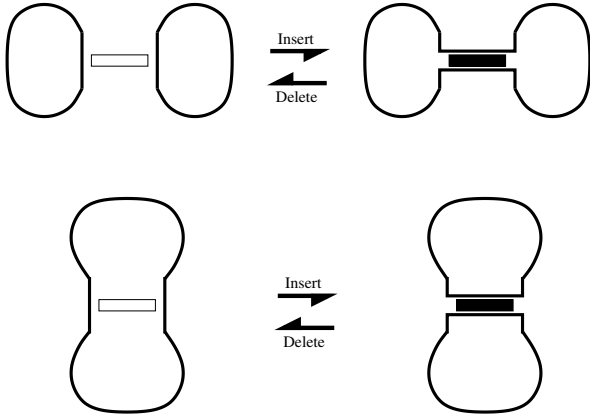


FIG. 1. Illustration of the basic update moves. The loop away from the operator is not drawn in register with the discrete space-time lattice which makes the point that the change in loop number  $n_l$  during these updates are purely determined by geometrical considerations.

In our implementation of the algorithm, we propose insertion of a non-identity operator on a random bond at a time slice that has an identity operator, and deletion

of the (non-identity) operator if the time slice already has a non-identity operator. The key step in the the update is the calculation of the change in number of loops due to insertion or deletion of an operator. The purely loop-geometric aspect of this calculation is sketched in Fig. 1. This is carried out algorithmically in the following way:

- **Insertion:** If two space-time points are on the same loop, the insertion of a non-identity operator at these two points splits the loop into two ( $n_l \rightarrow n_l + 1 \implies \delta(n_l) = 1$ ). Conversely, if they are on different loops, the two loops merge into one on inserting an operator ( $n_l \rightarrow n_l - 1 \implies \delta(n_l) = -1$ ). This has been shown schematically in Fig. 1. The Metropolis probability for acceptance of the insertion update:

$$P_{\text{accept}}(\text{identity} \rightarrow \text{non-identity}) = \min\left[\frac{\beta J N_b}{N(M-n)} N^{\delta(n_l)}, 1\right], \quad (3)$$

where  $N_b$  is the total number of bonds in the lattice.

- **Deletion:** If on an operator vertex, all the four legs [2] of the operator vertex touch the same loop, the removal of the operator results in splitting of the loop into two ( $n_l \rightarrow n_l + 1 \implies \delta(n_l) = 1$ ). On the other hand if two different loops touch the two sides of the operator vertex, the deletion of the operator results in merging of the two loops ( $n_l \rightarrow n_l - 1 \implies \delta(n_l) = -1$ ). This has been shown schematically in Fig. 1. The Metropolis probability for acceptance of the insertion update is given by:

$$P_{\text{accept}}(\text{non-identity} \rightarrow \text{identity}) = \min\left[\frac{N(M-n+1)}{\beta J N_b} N^{\delta(n_l)}, 1\right], \quad (4)$$

where  $N_b$  is the total number of bonds in the lattice.

- **Rewiring:** In the case of more than one mini-spin for higher symmetric representations, this update is carried out at the projection operator time slice. As shown in Fig 5 of the main manuscript, this kind of update can increase or decrease the number of loops. Therefore the update is accepted with the Metropolis probability of

$$P_{\text{accept}}(\text{rewire}) = \min[N^{\delta(n_l)}, 1] \quad (5)$$

In order to determine if two space-time points are on the same loop, we grow the loop starting from one of the points and check if the second point lies on that loop. We do this by storing the operator string as a linked-list data structure which correctly stores the connections

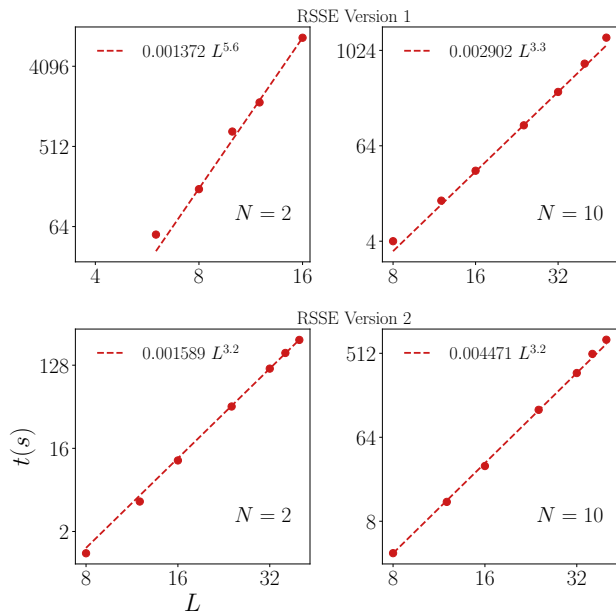


FIG. 2. Time taken for  $10^5$  Monte Carlo steps as a function of system size,  $L$ , with  $\beta = L$  plotted on a log-log plot and fitted to a power-law for  $N = 2$  (long loop phase) and  $N = 10$  (short loop phase). One expects that operator string length,  $M \propto L^2\beta = L^3$ . Version 1 of the resummed-SSE (RSSE) algorithm scales as  $O(M)$  only in the short loop phase, while version 2 scales this way in both phases. (here version 1 and 2 are as explained in the text)

between the various non-identity operators (as in Fig. 7, also see Fig. 57 of Ref. [1] and associated text for a discussion on this). This computation is time consuming in the long loop (magnetic) phases, but is very efficient in short-loop phases. We use two different implementations of the algorithm in the main manuscript:

- *Version 1*: An insertion/deletion update is proposed at every time slice. Only in the short loop phase, does this version scale as  $O(M)$ , similar to standard SSE. In the long loop phase, however, one typically needs to grow loops of  $O(M)$  length to carry out each update, resulting in costly and hence not as efficient updates. The contrast in performance of this algorithm in the two kinds phases is shown in Fig. 2.
- *Version 2*: An update is proposed at a random time slice. The number of such updates per Monte Carlo step is determined by requiring that the number of sites touched while growing loops during each insertion/deletion operation is  $O(M)$ . Clearly, this update scales as  $O(M)$  in either phase (see Fig. 2). In the long loop phases, there are much fewer updates per Monte Carlo step leading to a less efficient update compared to the short loop phase. This up-

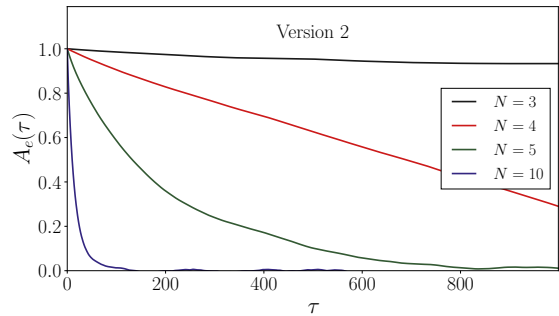


FIG. 3. Autocorrelation of the energy per unit site on a  $16 \times 16$  lattice measured after each Monte Carlo step using version 2 of our algorithm for  $N = 3, 4, 5, 10$ . The autocorrelations systematically get better as  $N$  increases.

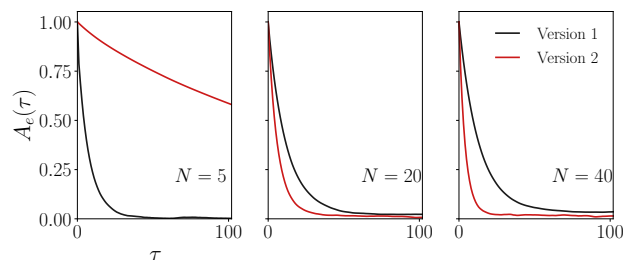


FIG. 4. Autocorrelation of the energy per unit site on a  $16 \times 16$  lattice measured after each Monte Carlo step for the two versions of the algorithm for  $N = 5, 20, 40$ . Version 1 does better for relatively smaller  $N$ .

date progressively does better as one goes deep into the short loop phase as can be seen from the autocorrelations of energy in Fig. 3.

Among the two versions, we find that version 1 performs better when not too deep in the short loop phase. As the loops get shorter, the number of updates per MC step increase for version 2, thus performing better than version 1. The data for  $N > 15$  has been collected using version 2 of the algorithm.

## OBSERVABLES

*Spin stiffness*: As mentioned in the main manuscript, the computation of spin stiffness in this algorithm is different from the computation in standard SSE. In standard SSE, the stiffness is computed using the winding of colored loops [1, 3]. For every off-diagonal operator, two differently colored loops touch both sides of the operator vertex. Each of these loops contribute to winding of their respective colors with opposite sign at this vertex. If these loops instead have the same color, i.e. the operator is diagonal, the contribution to winding of that color cancels out. Winding loops occur in pairs with opposite

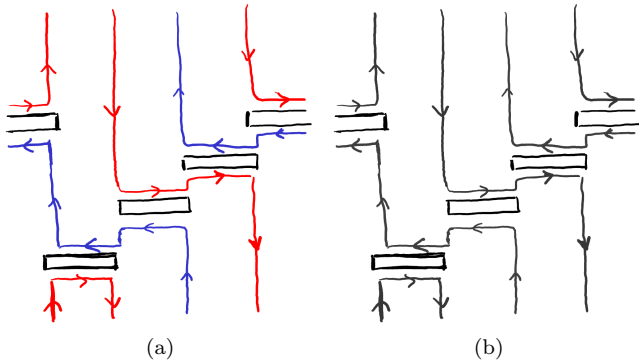


FIG. 5. A configuration of a pair of winding loops in (a) SSE and (b) resummed-SSE. In SSE, contributions to winding come from a string of off-diagonal operators. In such configurations, loops of two different colors touch the operators on the two sides of each operator vertex along the string of operators. Hence, winding loops always appear in pairs, each winding in opposite directions.

signs whenever there is a string of off-diagonal operators as shown in Fig. 5(a).

In our algorithm, there is no notion of color or diagonal/off-diagonal bonds. Therefore we proceed as follows: we seek to find the fraction of colored loops, upon coloring back the uncolored loop configuration, that would have contribute to stiffness or (colored) winding fluctuations as described in the previous paragraph. Consider a pair of winding loops,  $l_1$  and  $l_2$ , with a signed winding of  $\mathcal{W}$  and  $-\mathcal{W}$  respectively (the number of times they wind around the spatial periodic boundary condition; assigning a sign to the winding is possible on bipartite lattices since the loops are “orientable” as shown in Fig. 5) in some configuration. Now, imagine coloring this pair of winding loops. Thus, the winding of color  $\alpha$  in terms of the uncolored loop windings ( $\mathcal{W}$ ) for this pair of loops  $l_1$  and  $l_2$  is:

$$\mathcal{W}_\alpha = [n_\alpha(l_1) - n_\alpha(l_2)]\mathcal{W} \quad (6)$$

where  $n_\alpha(l) = 1$  if loop  $l$  is of color  $\alpha$ , otherwise  $n_\alpha(l) = 0$ . It is clear that  $\mathcal{W}_\alpha$  is non-zero only when exactly one of the loops has color  $\alpha$ . The number of ways in which exactly one of the two loops has color  $\alpha$  is  $2(N-1)$ . If one now averages over all possible colorings of  $l_1$  and  $l_2$ , the fraction of loop colorings that contribute to winding of color  $\alpha$  is  $\frac{2(N-1)}{N^2}$ . Therefore:

$$\overline{(\mathcal{W}_\alpha)^2} = \frac{2(N-1)}{N^2}\mathcal{W}^2 \quad (7)$$

where  $\overline{\mathcal{W}_\alpha^2}$  denotes the average of  $\mathcal{W}_\alpha^2$  over all possible loop colorings of  $l_1$  and  $l_2$ . We further average over the colors (for better statistics) to arrive at  $\overline{\mathcal{W}_c^2} = \frac{1}{N} \sum_\alpha \overline{\mathcal{W}_\alpha^2}$ . The uncolored winding squared for  $l_1$  and  $l_2$  is simply  $\mathcal{W}_u^2 = 2 \times \mathcal{W}^2$ . Note that the factor in Eq. 7 are just

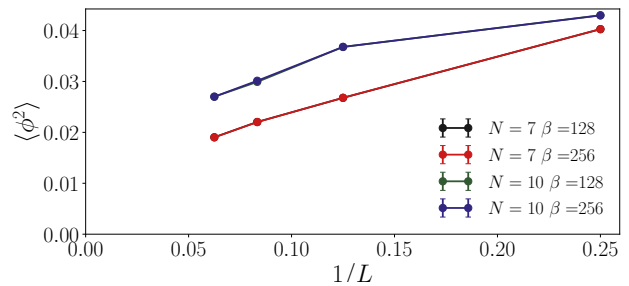


FIG. 6. The VBS order parameter,  $\langle \phi^2 \rangle$ , plotted as a function of inverse system size for two different inverse temperatures,  $\beta = 128$  and  $\beta = 256$ . The curves for  $\beta = 128$  and  $\beta = 256$  lie right on top of each other showing convergence with temperature.

a function of  $N$  and thus remains the same for all pairs of winding loops. Therefore, the squared winding of uncolored loops in terms of the average squared winding of colored loops is given by the following relation:

$$\mathcal{W}_u^2 = \frac{N^2}{(N-1)} \overline{\mathcal{W}_c^2} \quad (8)$$

*VBS order parameter:* In the VBS phase, the Fourier transform of the equal time correlator of the bond operator  $B_\lambda(\mathbf{r})$  as defined in the main text,  $\tilde{C}_{\phi_\lambda^2}(\mathbf{k}) = \frac{1}{N^s} \sum_{\mathbf{r}} e^{i\mathbf{k}\cdot\mathbf{r}} \langle B_\lambda(\mathbf{0})B_\lambda(\mathbf{r}) \rangle$  has a Bragg peak at  $\mathbf{k} = \pi\hat{e}_\lambda$ , where  $\hat{e}_x = (1,0)$  and  $\hat{e}_y = (0,1)$ . The height of this peak is the square of the VBS order parameter,  $\langle \phi_\lambda^2 \rangle = \tilde{C}_{\phi_\lambda^2}(\pi\hat{e}_\lambda)$ . The correlator of the bond operator as defined in the main manuscript is measured in the same way as in standard SSE.

## TEMPERATURE DEPENDENCE OF OBSERVABLES

As highlighted in the main text, our algorithm is a finite- $T$  generalization of valence bond  $T = 0$  projector QMC algorithm [4, 5] and its continuous- $N$  variant [6] but with periodicity in imaginary time and without being in total  $S = 0$  sector. Our algorithm is a generalization in the sense that it retains the (uncolored) “valence bond” spirit even though not being restricted to the total  $S = 0$  sector. There can for example be uncolored loops that loop non-trivially along the imaginary time direction (e.g. on sites 1 and 4 in Fig. 7. At low enough temperatures in an antiferromagnet, such time-winding loops however will be extremely unlikely even though in principle allowed, which will practically keep the ensemble in total  $S^z = 0$  sector. In the next section, we will see that these cases actually correspond to “monomer” defects in valence bond configurations.

We now show how finite temperature data converges towards zero temperature. We choose  $\beta = 128J$  for

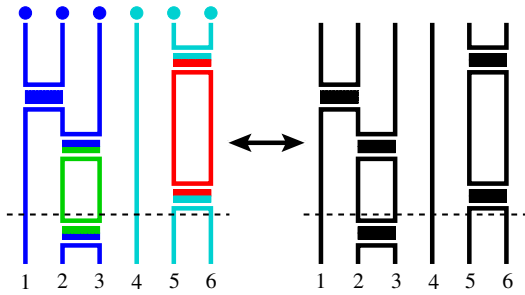


FIG. 7. An illustrative operator string configuration for a) standard SSE, and b) for resummed SSE. The dashed horizontal line depicts a typical time slice in the imaginary time direction.

studying groundstate properties at  $N = 7, 10, 13$ . Fig. 6 shows convergence of the VBS order parameter as a function of temperature for  $N = 7, 10$ .

### APPROACH TO QDM HILBERT SPACE AT LARGE $N$

For this discussion, we start by asking what each time slice represents in the uncolored loop ensemble. In the colored loop ensemble, each time slice represents a definite spin state, i.e. each site of the lattice has a definite spin or color  $\prod_i \otimes |\alpha_i\rangle$  at all time slices. After resumming, the uncolored loop is a “superposition” over the colors in space-time. What is the effect of this superposition at some chosen time slice. Each time slice makes a slice perpendicular to the imaginary time direction in the uncolored loop gas configuration as shown by the dashed line in Fig. 7. Under this, the lattice gets subdivided into a disjoint sets of sites with the following properties: a) two sites from the same set are connected by the same uncolored loop, and b) two sites from two different sets are not connected by any loop. Thus, sites from the same set upon coloring back will necessarily have the same color, while sites belonging to different sets need not have the same color, as can be seen on the left panel of Fig. 7. There can be sets with only one site at finite- $T$ , e.g. sites 4 and 6 in Fig. 7 at the dashed time slice.

Any given set of sites with the same color upon coloring back may now be interpreted as follows: It is the *overlap* of two appropriate states. This is essentially a generalization of the “central” time slice interpretation in the  $T = 0$  valence bond projector QMC as an overlap of two valence bond states while stochastically estimating various physical observables. (e.g. see the central time slice represented as a dashed line in Fig. 91 of Ref. [1]). For the base cases of

- 1) a set with one site ( $i$ ), the two appropriate states could be  $|s_i^x = \frac{1}{2}\rangle \equiv \frac{1}{\sqrt{2}}(|s_i^z = \frac{1}{2}\rangle + |s_i^x = -\frac{1}{2}\rangle)$  or any other state in the  $xy$ -plane of the Bloch

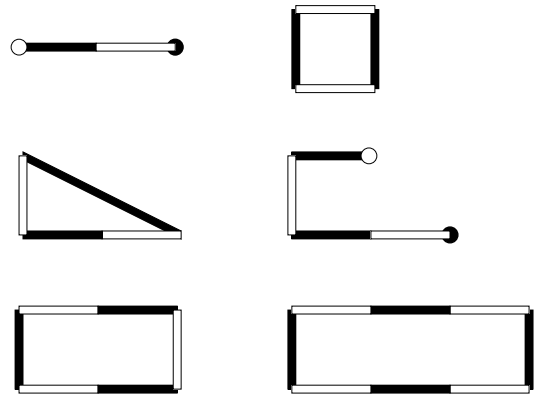


FIG. 8. Examples of disjoint sets with more than two sites. The top left and middle row are examples that violate the QDM Hilbert space condition, while the other examples respect this condition.

sphere, suitably generalized to any  $N$  (say  $|\bullet_i\rangle \equiv \frac{1}{\sqrt{N}} \sum_\alpha |\alpha_i\rangle$ ). Upon overlapping them  $\langle \bullet_i | \bullet_j \rangle$ , we indeed get the same color upon coloring back at this single site with each coloring being equally weighted, i.e.  $\langle \bullet_i | \bullet_j \rangle = \frac{1}{N} \sum_\alpha \langle \alpha_i | \alpha_i \rangle$ . This case arises because the uncolored loop ensemble is at finite- $T$ .

- 2) a set with two sites ( $i$  and  $j$ , not necessarily nearest neighbor), the two appropriate states are singlets on the bond formed by  $i$  and  $j$ ,  $|-\!_{ij}\rangle \equiv \frac{1}{\sqrt{2}} \sum_\alpha |\alpha_i \alpha_j\rangle$ . Upon overlapping them  $\langle -\!_{ij} | -\!_{ij} \rangle$ , we indeed get the same color upon coloring back at this set of two sites with each coloring being equally weighted, i.e.  $\langle -\!_{ij} | -\!_{ij} \rangle = \frac{1}{N} \sum_\alpha \langle \alpha_i \alpha_j | \alpha_i \alpha_j \rangle$ .

This interpretation carries over to sets with more number of sites. They correspond to a “transposition graph” due to the overlap of two dimer or singlet configurations that are compatible with the geometry of the set of sites. From this point of view, the first point in the list above on the case of a set with a single site corresponds to a monomer defect at the corresponding time slice. Several examples of such disjoint sets with more than two sites interpreted as overlaps of two singlet configurations are shown in Fig. 8. For the case of the top left example in Fig. 8, the two appropriate states are the following configurations with monomers,  $|-\!_{ij}\rangle \otimes |\bullet_k\rangle$  and  $|\bullet_i\rangle \otimes |-\!_{jk}\rangle$ .  $i, j, k$  is, say, a linear indexing from left to right of the three sites in this example, and the black monomer and dimer represents one of these two states, while the white monomer and dimer represents the other state. Again, upon overlapping these two states, we indeed get the same color upon coloring back at this set of three sites with each coloring being equally weighted, i.e.  $\langle (-\!_{ij}) \otimes (\bullet_k) | (\bullet_i) \otimes (-\!_{jk}) \rangle = \frac{1}{N^2} \sum_\alpha \langle \alpha_i \alpha_j \alpha_k | \alpha_i \alpha_j \alpha_k \rangle$ . For the case of top right example in Fig. 8, the two appro-

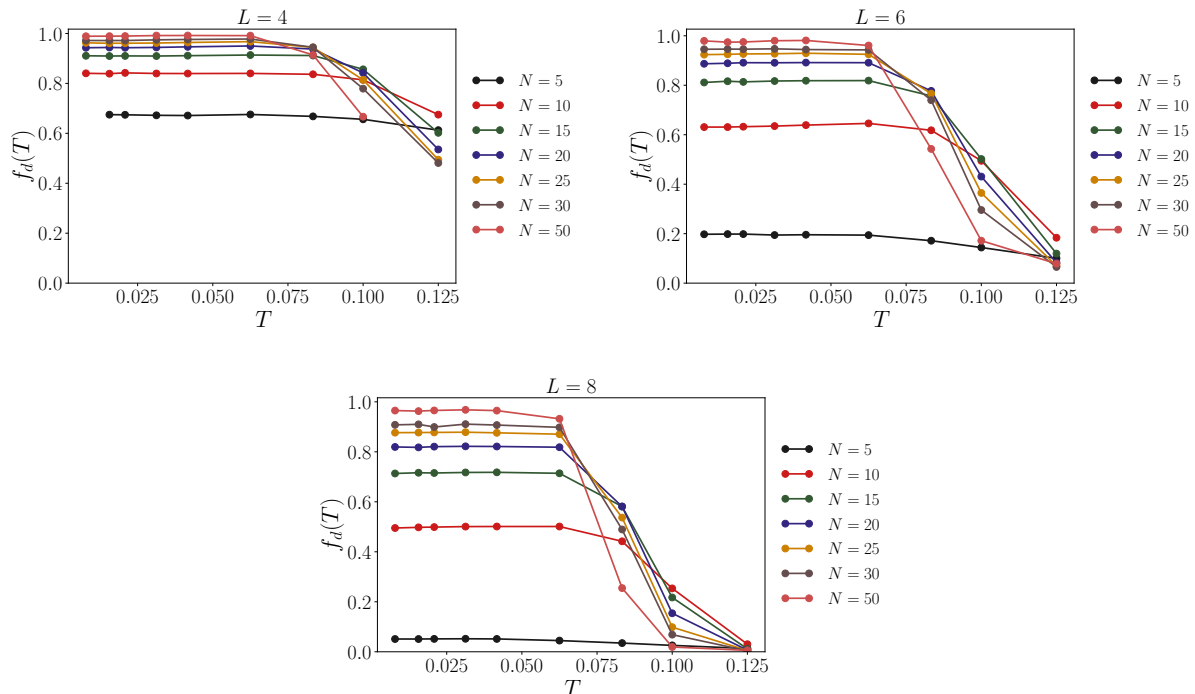


FIG. 9. The fraction  $f_d$  of typical time slices which are consistent with the QDM Hilbert space is shown above vs. temperature  $T$  for several values of  $N$ . We see that there is a non-negligible violations of the QDM Hilbert space condition already at  $L = 8$  for moderately large values of  $N$ . This suggests that approaching the perturbative neighborhood of the QDM Hilbert space at large system sizes for  $SU(N)$  magnets might require really large values of  $N$ . Formally, this approach is expected for  $N \gg 1$ .

appropriate states are the following singlet configurations,  $|\!-\!_{ij}\rangle \otimes |\!-\!_{kl}\rangle$  and  $|\!-\!_{kl}\rangle \otimes |\!-\!_{li}\rangle$ .  $i, j, k, l$  is, say, a clockwise indexing of the four sites in this example, and the black dimers represent one of these two states, while the white dimers represent the other state. Again, upon overlapping these two states, we indeed get the same color upon coloring back at this set of four sites with each coloring being equally weighted, i.e.  $(\langle\!-\!_{ij}\rangle \otimes \langle\!-\!_{kl}\rangle | \langle\!-\!_{jk}\rangle \otimes |\!-\!_{li}\rangle) = \frac{1}{N^2} \sum_{\alpha} \langle \alpha_i \alpha_j \alpha_k \alpha_l | \alpha_i \alpha_j \alpha_k \alpha_l \rangle$ . For sets with even more sites as in the other examples of Fig. 8, a similar interpretation can be applied by generalizing the above steps appropriately.

As mentioned earlier, this is quite analogous to the time slice interpretation in the  $T = 0$  valence bond projector QMC. In the standard implementation of  $T = 0$  valence bond projector QMC where one does not have any periodicity in imaginary time but rather “open” time boundary conditions, one usually does the updates in the spin basis using standard SSE updates *à la* Sandvik and Evertz. We are extending the same time slice interpretation to the finite- $T$  case now with periodicity in imaginary time such that all time slices have the same status. Then, the corollary follows that for the case of  $T = 0$  as well, one can directly work with the uncolored loops, if so one chooses, using the resummation-based updates that is the subject of this paper.

Based on the above interpretation, we now quantify the approach to the QDM Hilbert space as follows: after equilibration or warm-up phase of the QMC simulation, for a typical time slice of the uncolored loop configuration, we construct the disjoint sets with sites that lie on the same uncolored loop. Then, we check if each disjoint set is compatible with the overlap of two nearest-neighbor dimer tilings or not, since the standard QDM Hilbert space contains only nearest-neighbor dimers with the constraint that no two dimers can meet at a site. If all the disjoint sets at a typical time slice are compatible with such nearest-neighbor dimer tiling overlaps, then the time slice is in the QDM Hilbert space. We collect statistic on this for several sizes and values of  $N$  as shown in Fig. 9. We see that uncolored loop ensemble starts approaching the QDM Hilbert space as  $N$  gets large, and  $T$  gets small. However, we note that there is a system size dependence to this, and for thermodynamically large systems, one might have to go to really large  $N$  or really low  $T$  to be in the perturbative neighborhood of the QDM Hilbert space. E.g., for  $N = 15$  and  $L = 8$ , there is already a 30% violation to the QDM Hilbert space condition, and the severity of such violations will only get worse as system size increases simply due to entropic reasons, i.e. there are more regions available in the lattice as system size increases where violations may occur.

- 
- [1] A. W. Sandvik, in *Lectures on the Physics of Strongly Correlated Systems Xiv: Fourteenth Training Course in the Physics of Strongly Correlated Systems*, American Institute of Physics Conference Series, Vol. 1297, edited by A. Avella and F. Mancini (2010) pp. 135–338, arXiv:1101.3281 [cond-mat.str-el].
- [2] Our operator vertex has four legs since we are working with a two spin interaction. For other interactions with more number of spins, e.g. the  $Q$ -term, the full operator vertex can be treated as multiple four legged operator vertices at the same time slice.
- [3] A. W. Sandvik, Phys. Rev. B **56**, 11678 (1997).
- [4] A. W. Sandvik, Phys. Rev. Lett. **95**, 207203 (2005).
- [5] A. W. Sandvik and H. G. Evertz, Phys. Rev. B **82**, 024407 (2010).
- [6] K. S. D. Beach, F. Alet, M. Mambrini, and S. Capponi, Phys. Rev. B **80**, 184401 (2009).